catalysts

MDPI

Article

Effect of Heating Rate on the Photocatalytic Activity of Ag–TiO_2 Nanocomposites by One-Step Process via Aerosol Routes

Kusdianto Kusdianto [1], Meditha Hudandini [2], Dianping Jiang [3], Masaru Kubo [2] and Manabu Shimada [2,*]

[1] Department of Chemical Engineering, Institut Teknologi Sepuluh Nopember (ITS), Kampus ITS Sukolilo, Surabaya 60111, Indonesia; kusdianto@chem-eng.its.ac.id
[2] Chemical Engineering Program, Graduate School of Advanced Science and Engineering, Hiroshima University, 1-4-1, Kagamiyama, Higashi-Hiroshima, Hiroshima 739-8527, Japan; d213956@hiroshima-u.ac.jp (M.H.); mkubo@hiroshima-u.ac.jp (M.K.)
[3] Department of Chemical Engineering, Graduate School of Engineering, Hiroshima University, 1-4-1, Kagamiyama, Higashi-Hiroshima, Hiroshima 739-8527, Japan; kyou.dianping@aist.go.jp
* Correspondence: smd@hiroshima-u.ac.jp

Abstract: Ag–TiO_2 nanocomposite films, based of Ag and TiO_2 nanoparticles, were fabricated in a one-step aerosol route employing the simultaneous plasma-enhanced chemical vapor deposition and physical vapor deposition systems. The as-fabricated films were subjected to different heating rates (3 to 60 °C/min) with a constant annealing temperature of 600 °C to observe the significant changes in the properties (e.g., nanoparticle size, crystalline size, crystallite phase, surface area) toward the photocatalytic performance. The photocatalytic activity was evaluated by the measurement of the degradation of a methylene blue aqueous solution under UV light irradiation, and the results revealed that it gradually increased with the increase in the heating rate, caused by the increased Brunauer–Emmett–Teller (BET) specific surface area and total pore volume.

Keywords: plasma-enhanced chemical vapor deposition; physical vapor deposition; heating rate; annealing temperature; organic material degradation

Citation: Kusdianto, K.; Hudandini, M.; Jiang, D.; Kubo, M.; Shimada, M. Effect of Heating Rate on the Photocatalytic Activity of Ag–TiO_2 Nanocomposites by One-Step Process via Aerosol Routes. *Catalysts* **2022**, *12*, 17. https://doi.org/10.3390/catal12010017

Academic Editors: Detlef W. Bahnemann, Wonyong Choi, Ioannis Konstantinou, Ewa Kowalska, Magdalena Janus, Vincenzo Vaiano and Zhi Jiang

Received: 25 November 2021
Accepted: 21 December 2021
Published: 24 December 2021

1. Introduction

Environmental problem and energy shortage are a great issue in many nations and must be efficiently handled, especially for those related to the waste treatment to decrease the operation cost and mitigate the risk to the society. In the case of liquid waste, wastewater containing organic compounds emitted from various sources (e.g., textile industries) is harmful to mankind. Using the bio-degradation method to decompose these pollutants is often very slow and ineffective. Photocatalytic utilization of semiconductor materials for the degradation of organic pollutants has shown significant results compared to the conventional chemical oxidation methods for the degradation of organic pollutants [1].

Research of TiO_2 has been extensively performed due to its low-cost, versatility, non-toxicity, high physical and chemical stability, among other photocatalytic materials [2,3]. TiO_2 can be utilized as a photocatalyst for the degradation of these organic pollutants. TiO_2 is known to have three crystalline phases of anatase, rutile, and brookite, of which anatase is known to have the highest photocatalytic performance [2,4–6]. However, with a band gap of 3.2 eV, the utilization is somewhat limited because of the fast electron-hole recombination that is likely to occur [6,7]. Suppressing this disadvantage is possible by several methods such as loading metal/non-metal ions, dye functionalization, or the growth of noble metals on the surface of TiO_2 [8]. One metal that can be loaded is Ag, under UV light irradiation, which acts as an electron sink of the excited electrons from the valance band (VB) of TiO_2 that can extend the lifetime of electron-hole separation [4,7]. Such a phenomenon can be explained because TiO_2 has a higher fermi level compared to Ag, which indulges the electron transfer toward Ag. As the fermi level comes to the same range, the Schottky barrier would form, which can improve the electron-hole separation [9].

Further enhancement is possible by obtaining the mixture phase of anatase–rutile TiO_2, which has been reported to form a heterojunction that increases the photocatalytic activity due to the optimized charge carrier separation [3]. There are still several characteristics that influence the activity of a photocatalyst such as the crystallinity, crystal phase, particle size, surface area, and several others that can be altered based on post processing heat treatments [6,10] or even added materials [3].

Several studies have reported that post annealing heat treatment can be applied to enhance the crystallinity of TiO_2 nanoparticles, which gives a better performance [3,11]. In the annealing process, the heating rate has been observed to influence the grain growth [12], crystal size [5], and crystal orientation [13] of the nanoparticles. Alternation of this parameter has the potential to optimize the activity of the nanoparticles. Dikici et al. [6] reported for TiO_2 powders that with an increase in heat rate (1 °C/min), the X-ray diffraction (XRD) results showed a shift in anatase phase to a higher degree, which is caused by the lattice strain. There was no change in morphology and size distribution. Furthermore, the highest photocatalytic activity was for a heat rate of 1 °C/min that had high crystallinity. Mansour et al. [11] tried to estimate the crystallization process of amorphous TiO_2 by differential scanning calorimetry (DSC) with different heating rates and reported that an increase in the heat rate shifts the optimum crystallization temperature to a higher temperature. These results show how significant the effect of the post annealing heating rate is toward the characteristics and functionality of the produced nanoparticles.

Not many have approached the influence of different heating rate in the annealing process for Ag–TiO_2 nanocomposites, which makes it intriguing for further discussion and investigation. Previously, we fabricated Ag–TiO_2 with the influence of different annealing temperatures that unveiled a change in the nanoparticle size, crystallite size, and crystalline phase, which influenced the photocatalytic activity for the degradation of methylene blue (MB) under UV light irradiation [10]. In this paper, the fabrication of a Ag–TiO_2 nanocomposite thin film was carried out by a one-step deposition method consisting of plasma enhanced chemical vapor deposition (PECVD) and physical vapor deposition (PVD) systems; subsequently, heat treatment with different heating rates was employed. The characteristics of the produced nanocomposite thin film with the effect of the heating rate can be elucidated regarding the morphology, size, thickness, and crystallinity. Furthermore, the correlation of these characteristics and the photocatalytic activity of the nanocomposite toward the degradation of MB as a model organic pollutant can also be explained.

2. Results and Discussions

2.1. Heating Rate Effect on the Surface Morphology and Thickness of the Ag–TiO_2 Nanocomposite Film

In our previous study [10], we confirmed the effect of the annealing temperature toward the morphology, which showed larger and thinner nanoparticles with the increase in annealing temperature. The change in annealing temperature also showed significant differences on the properties of crystallite size and phase content, and consequently, the photocatalytic performance of the nanocomposite films.

Figure 1 shows the SEM images showing the top view (insets) and cross-sectional areas of the nanocomposite films as deposited and annealed at 600 °C at different heating rates of 3, 5, 10, 30, and 60 °C/min. The results indicate that the GMD of particles in the as-deposited film was 13 nm, which was less than those of the particles in all of the experimental series at different heating rates (Figure S1). The increase in particle size after annealing is closely related to the particle's mobility, an increase in the kinetic energy of the particles, and the diffusion rate, which resulted in the coalescence of small particles forming larger ones [14]. However, no significant difference was observed for the GMD of nanoparticles after heating at various rates, with GMD values of 22, 25, 24, 20, and 22 nm for heating rates at 3, 5, 10, 30, and 60 °C/min, respectively (Figure S2). This result indicates that the change in the heating rate from 3 to 60 °C/min does not significantly affect the particle size of nanocomposite films. Guhel et al. [15] have reported that the

particle size of cerium dioxide does not change after subjecting it to various heating rates, albeit the heating rate affects the domain (the regions surrounded by the cracks) diameter. The domain diameter decreases with the increase in the heating rate, caused by the strain effect.

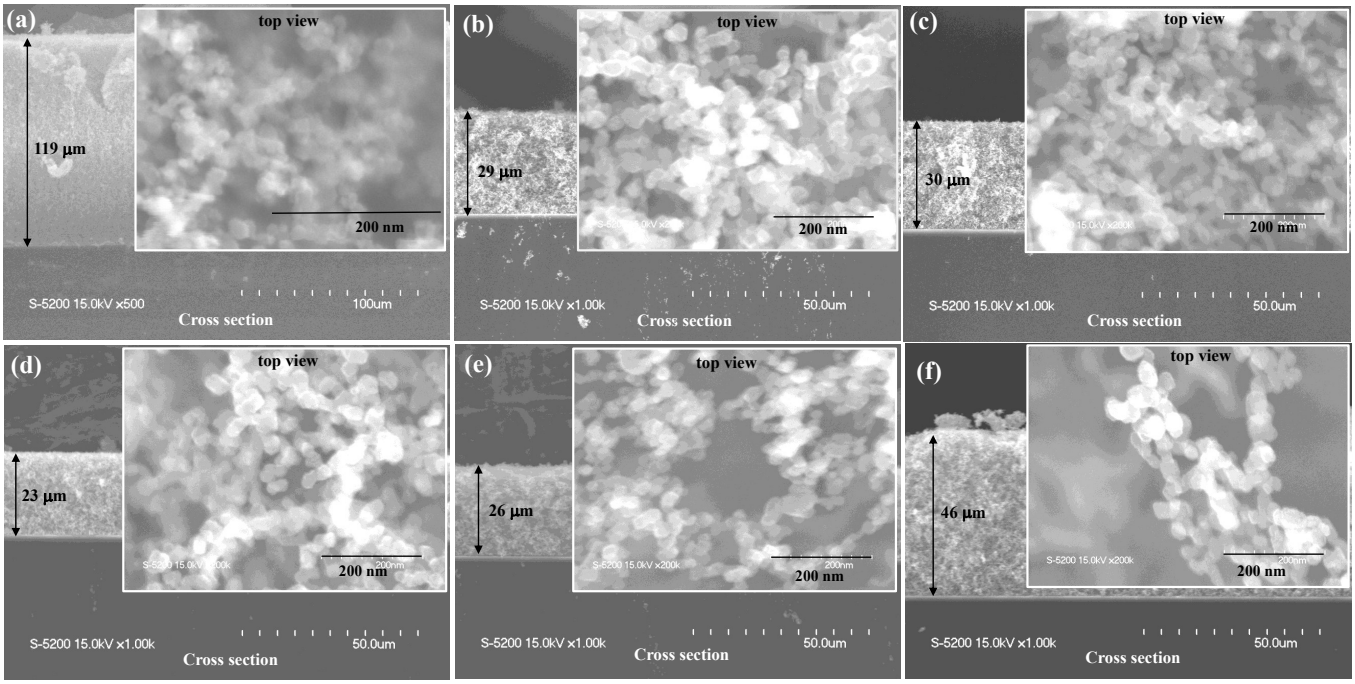

Figure 1. SEM images on the top views and cross section areas of nanocomposite thin films with a different heating rate: as-deposited film (**a**), 3 °C/min (**b**), 5 °C/min (**c**), 10 °C/min (**d**), 30 °C/min (**e**), and 60 °C/min (**f**). Annealing temperature was kept constant at 600 °C.

These results show that the relative thickness decreases with the applied heat treatment. The densification of the film after annealing was closely related to the release or dehydration of residual hydroxyl group by the heat [16]. The relative thickness was obtained from the measured thickness of the annealed film divided by the thickness of the as-deposited film. There was no significant difference from 3 to 30 °C/min. Moreover, the relative thickness increased from 30 to 60 °C/min (see Figure S2). The relative thickness gradually increased at a heating rate of 60 °C/min even though the GMD of those particles did not significantly change, possibly caused by a relatively large temperature gradient within the nanocomposite structure at a high heating rate [15]. In addition, a high heating rate may lead to a short calcination process, leaving insufficient time for all nanoparticles in the main framework to coalesce; thus, the film structure is thicker than that at low heating rates.

2.2. Crystalline Phase of Ag–TiO_2 Nanocomposite Film

XRD patterns of the nanocomposite films annealed at 600 °C at a heating rate from 3 to 60 °C/min, bare Si substrate, and the as-deposited nanocomposite film are shown in Figure 2. The peak at 2θ = 33° corresponded to the Si substrate used [17]. The XRD pattern of the as-deposited film showed only the peak for Si, which indicates an amorphous nanocomposite film. However, the amorphous phase is then transformed into a mixture of anatase–rutile crystalline phase after annealing at different heating rates. The XRD patterns of all nanocomposite films exhibited similar diffraction peaks, corresponding to the anatase–rutile mixed phase. The diffraction peaks observed at 25.4, 37.5, 38.3, 39.1, 48.5, 54.8, 55.5° corresponded to the 101, 103, 004, 112, 200, 105, and 211 diffraction peaks of anatase TiO_2, respectively [2,18,19]. The highest intensity at 2θ = 25.4° indicated that anatase (101) is the most dominant crystal phase of the nanocomposite films, which was confirmed by the selected-area electron diffraction (SAED) pattern (Figure S3). On the other

hand, the diffraction peaks at 2θ = 27.8, 36.6, 39.3, 41.7, and 57.1° corresponded to the 110, 101, 200, 111, and 220 diffraction peaks of rutile TiO_2, respectively [2,19]. Furthermore, the existence of Ag (2θ = 38.2 and 44.3°) cannot be confirmed by XRD, which can indicate the presence of highly dispersed Ag in the nanocomposite. In addition, there is the possibility of the overlapping peak of Ag with the anatase peak at 38.3°. Nonetheless, in our previous study [20], the existence of Ag was already confirmed by EDS mapping from the resulting TEM images.

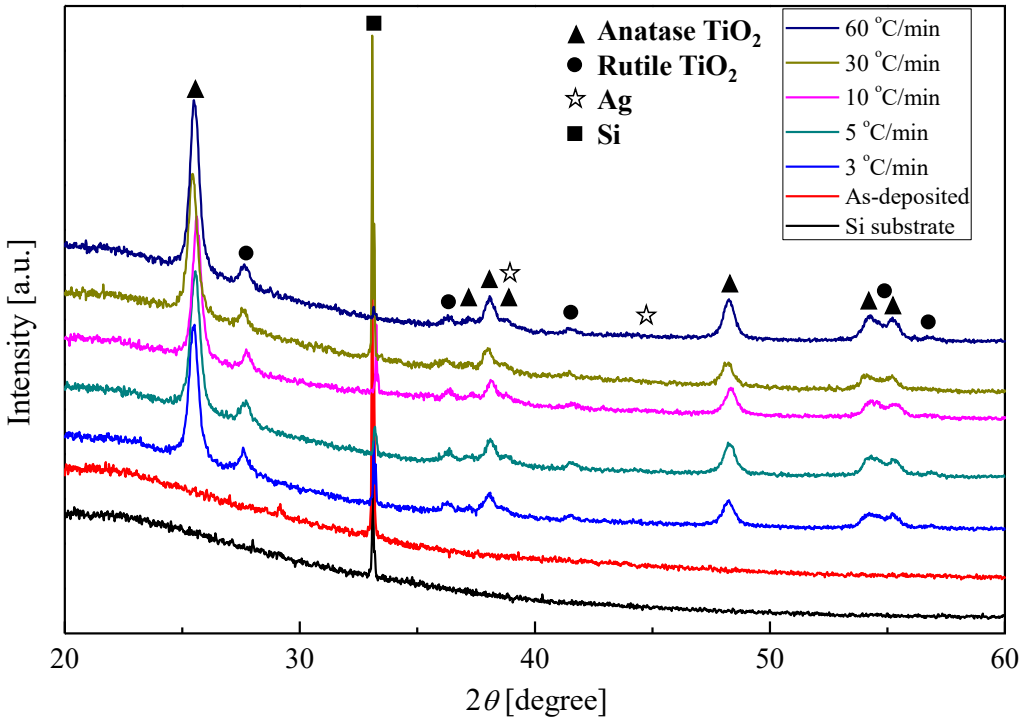

Figure 2. XRD patterns of TiO_2–Ag nanocomposite films annealed at 600 °C with heating rates of 3–60 °C/min including as-deposited.

The average crystallite size (Figure S4) of anatase and rutile was estimated by the Scherrer equation (Equation (3)) based on peaks at the lattice planes of 101 and 110 for anatase and rutile, respectively. No significant difference in terms of the crystallite sizes of anatase was observed at all of the heating rates (even though the crystallite size seems to slightly increase approximately 2 nm), with sizes ranging from 26 to 29 nm, indicating that the crystallite size of anatase is not affected by the change in the heating rates, even though the heating rate was increased up to 60 °C/min. Notably, a discrepancy was observed between our results and those reported by Tao et al. [21]: with the increase in the heating rate from 2 to 10 °C/min, the crystallite size of tantalum pentoxide decreased to approximately 4 nm. However, the crystallite size of rutile (31–45 nm) was clearly greater than that of anatase (Figure S4). The crystallite size of rutile decreased from a heating rate of 3 °C/min (41 nm) to 60 °C/min (32 nm), except for a heating rate of 5 °C/min. Moreover, the phase content of anatase and rutile in the mixed-phase structure can also calculated by Equation (4). Even with the application of different heating rates, the phase content of anatase and rutile appeared to be constant, in which the phase content of the nanocomposite was dominated by the anatase phase (~84%), while the phase content of rutile was estimated to be approximately 16% (Figure S5).

Considering the results reported in the previous paragraphs, the effect of the heating rate was thought to be less dominant compared with that of the holding time during annealing for the purpose of controlling the morphology and crystallite size of the nanocomposite film. To clarify this issue, a series of experiments at two heating rates (3 and 60 °C/min, respectively) with a short holding time (2 h) at an annealing temperature of 600 °C were

conducted. A slight difference was observed in the XRD patterns between the heating rates of 3 and 60 °C/min (Figure 3), even though a slightly higher intensity was observed at the high heating rate compared with that observed at the low heating rate. A small diffraction of rutile peak was observed at $2\theta = 27.8°$ in both spectra, indicating that the rutile phase was present in the nanocomposite after annealing at a short holding time of 2 h. However, the intensity of the diffraction peaks was less than that of the rutile diffraction peak at a holding time of 12 h during annealing (Figure 2). This result indicates that compared to the heating rate, the holding time predominantly controls the crystal phase of the nanocomposite.

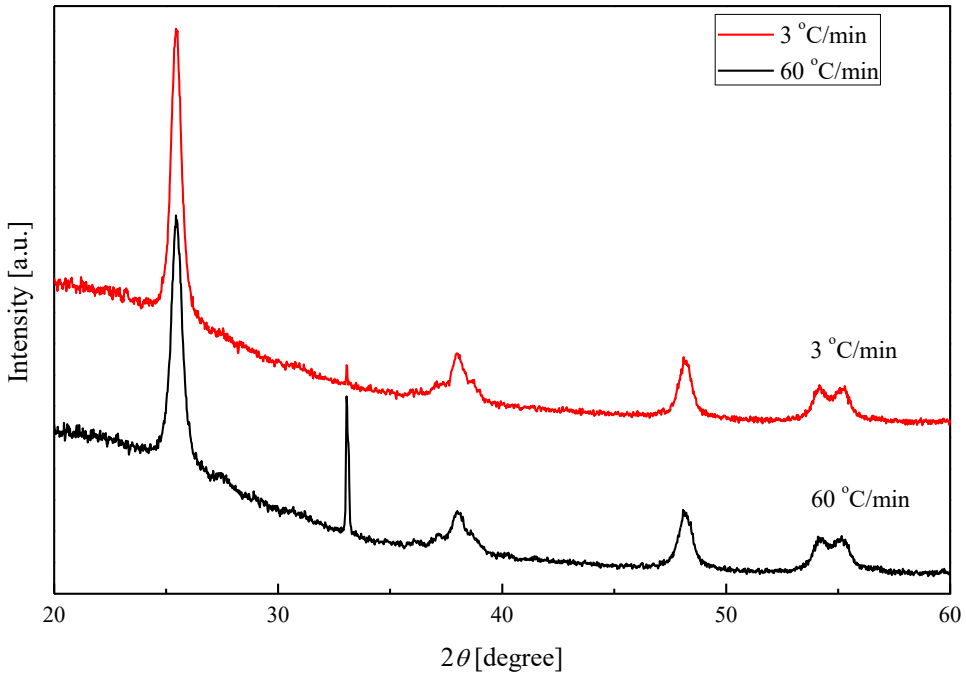

Figure 3. XRD patterns of the Ag–TiO_2 nanocomposite film annealed at 600 °C with heating rates of 3 and 60 °C/min. The holding time for annealing was maintained at 2 h.

2.3. Photocatalytic Activity Evaluation of Ag–TiO_2 Nanocomposite Films

The photocatalytic activity was assessed by the degradation of a MB aqueous solution under UV light irradiation. Figure S6 shows an example of the UV–Vis absorption spectra of MB (2 ppm) under UV light irradiation in the presence of the Ag–TiO_2 nanocomposite film after annealing at 600 °C and a heating rate of 60 °C/min. The absorption peak decreased with increasing irradiation time, indicating that MB undergoes photodegradation by the nanocomposite particles during UV light irradiation. The values obtained from the absorbance data (at a wavelength of 664 nm) were then converted into concentration and used to calculate the MB degradation efficiency using Equation (5) (Figure S7). Generally, the MB degradation efficiency increased with the irradiation time for across the whole series of experiments. Moreover, the MB degradation efficiency increased from 56% to 70% with the increase in the heating rate from 3 to 60 °C/min, respectively. High efficiency indicates good performance of the catalyst particles to degrade MB.

Photocatalytic activity was then determined by the measurement of the pseudo-first order rate constant (k) based on the equation of $\ln(C_0/C_t) = kt$. Figure 4a shows the plot of $\ln(C_0/C_t)$ as a function of irradiation time at different heating rates: With the increase in the heating rate, $\ln(C_0/C_t)$ values increase. The rate constants are obtained by measuring the slope of the fitted linear curves of $\ln(C_0/C_t)$ versus irradiation time (Figure 4b). With the increase in the heating rates, the rate constant gradually increases. The highest rate constant at a heating rate of 60 °C/min indicates the rapid degradation of MB and excellent photocatalytic activity.

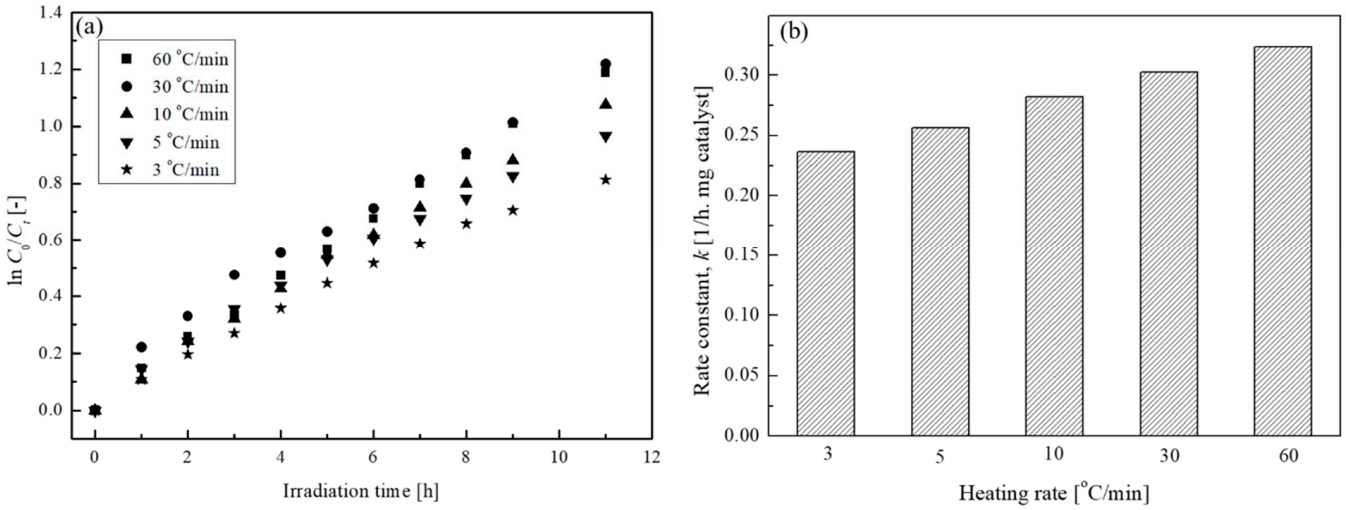

Figure 4. Photocatalytic activity of the Ag–TiO_2 nanocomposite films annealed at 600 °C with different heating rates: plots of ln C_0/C_t vs. irradiation time (**a**) and rate constants (**b**).

Typically, photocatalytic activity is affected by several parameters (e.g., SEM particle size, crystallite size, and phase content). However, no significant difference was observed in the obtained values, indicating that the increase in the photocatalytic activity cannot be related to those parameters. At this moment, the mechanism is not clear; nevertheless, one possibility for the photocatalytic activity enhancement at a heating rate of 60 °C is related to the different thickness among the films. As can be observed in Figure S2, a thicker film was observed at a heating rate of 60 °C/min compared with those observed at different heating rates (3–30 °C/min), permitting the increased possibility for the better contact between the catalyst particles and the probe dye molecules, resulting in the degradation of a large number of organic compounds. The enhanced photocatalytic activity at a high heating rate may also be related to the high crystallinity of the produced film, as observed by TEM analysis. High-resolution TEM images down to several nanometers revealed that a high rate (60 °C/min) leads to higher crystallinity compared with that observed at a low heating rate (5 °C/min), as reflected by the lattice spacing of the anatase or rutile phase (Figure 5). Based on XRD analysis, however, this detailed information about the crystalline lattice spacing was not observed (no significant difference was observed in the XRD results) as XRD exhibits limitations for the measurement of the bulk sample area. The high crystalline phase based on TEM observation is indicated by the entire area of the nanocomposite particles that is mostly occupied by the crystalline phase structure at high heating rates (only a small portion is imperfectly crystallized, as shown in Figure 5b). In contrast, Figure 5a shows a large part of the imperfectly crystallized phase structure at a low heating rate. The imperfectly crystallized part is thought to be related to the low crystallinity of the anatase phase; hence, the lattice spacing was not clearly observed. The smaller imperfectly crystallized part at a high heating rate is thought to exhibit higher crystallinity, which will contribute toward the enhancement of the photocatalytic performance for the produced nanocomposite film. TEM images revealed that the crystallite size of the nanocomposite was dominated by the diffraction peak of anatase (101), indicated by the existence of a lattice spacing of 0.35 nm. This result is in good agreement with those obtained from XRD and SAED analyses, while a lattice spacing of 0.24 nm is in agreement with the Ag (110) plane [22,23].

In addition, nitrogen adsorption–desorption isotherms analysis was employed to obtain detailed information about the surface area and pore volume of the produced nanocomposites after subjecting them to different heating rates (Figure 6). The fabricated nanocomposites exhibited Type II(b) isotherms, characteristic of a non-porous or macroporous adsorbent. Unrestricted multimolecular (multilayer) adsorption was observed at high P/P_o [24,25]. However, the produced particles in our case are thought to be non-porous,

not macroporous, particles. By definition, macroporous particles are particles with pore widths of greater than approximately 50 nm. Furthermore, multilayer adsorption occurs within a non-rigid aggregated particle, as indicated by the narrow hysteresis loop [24]. The BET surface area and pore volume values based on the nitrogen adsorption–desorption isotherm analysis clearly indicated that the values increased with the increase in the heating rate (Figure 7), with the exception of the pore volume at 5 °C/min, see the inset in Figure 7. Subsequently, the particle size was also estimated from the BET surface area using Equation (1) [24]:

$$d_p = \frac{6}{\alpha\rho} \quad (1)$$

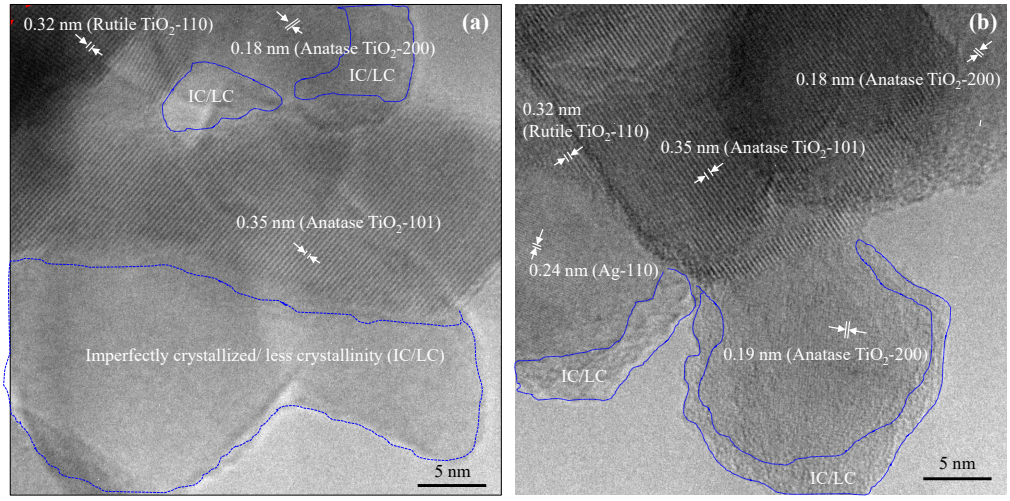

Figure 5. TEM images of the Ag–TiO_2 nanocomposite films annealed at 600 °C with heating rates of 5 °/min (**a**) and 60 °C/min (**b**). The holding time for annealing was maintained at 12 h.

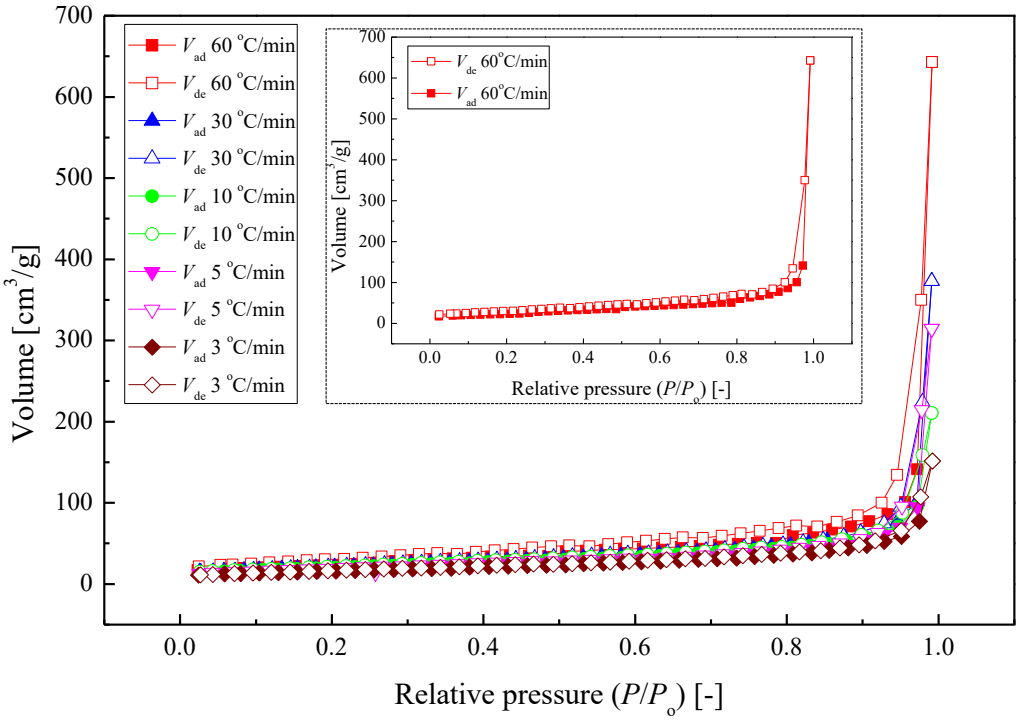

Figure 6. Nitrogen adsorption–desorption isotherms of the Ag–TiO_2 nanocomposite films annealed at 600 °C with heating rates of 3–60 °C/min.

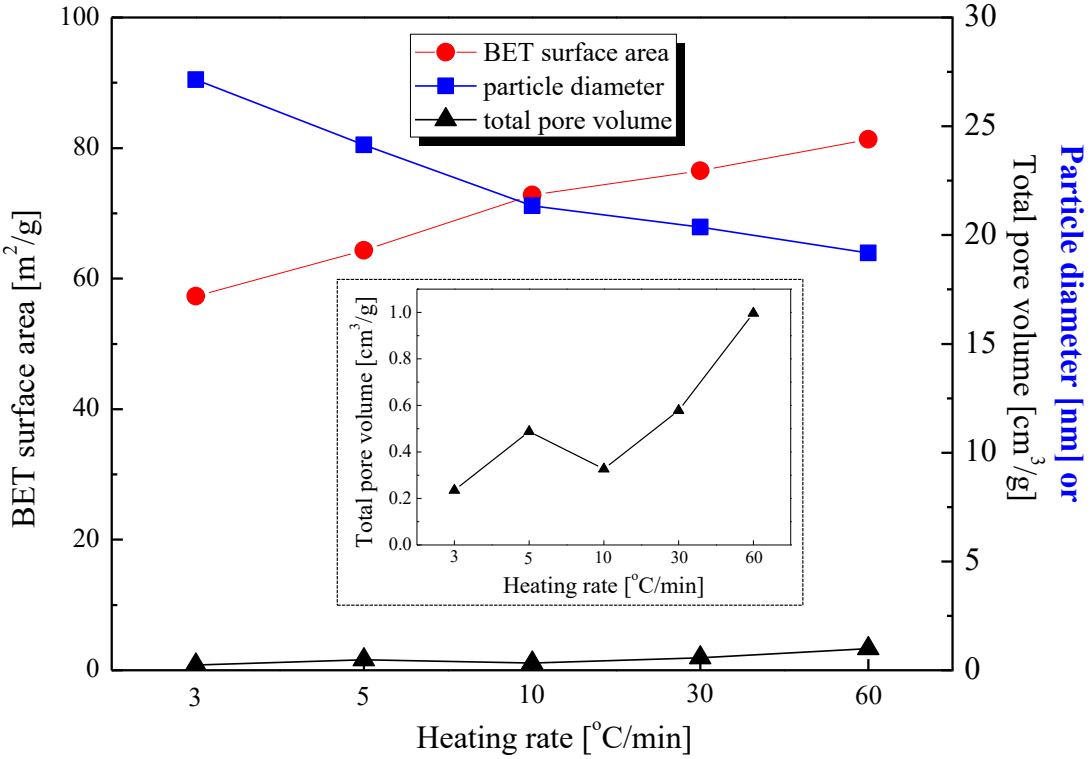

Figure 7. BET surface area, total pore volume, and particle diameter measured from the BET surface area data for the Ag–TiO_2 nanocomposite films annealed at 600 °C with heating rates of 3–6 °C/min.

Here, d_p, a, and ρ represent the geometrical particle size, specific surface area, and particle absolute density, respectively. The absolute density is obtained by the calculation of the density of the anatase–rutile mixed phase based on their phase content (estimated from XRD results), where the densities of anatase and rutile were 3.8 and 4.2 g/cm^3, respectively [24]. The estimation revealed that the BET particle size decreased with the increase in the heating rate (Figure 7). Based on these results, the enhanced photocatalytic activity is thought to be predominantly related to the increasing surface area and pore volume, resulting in the adsorption of a large number of dye molecules on the catalyst surfaces.

Moreover, a large pore volume permits the penetration of the dye molecules into deep areas of catalyst particles, producing reaction sites and affording high photocatalytic activity to degrade a number of molecules of the organic compound. Table 1 shows the summarization of the crystalline phase, GMD of the nanoparticles, crystallite size of anatase and rutile phases and their content, relative thickness, and the reaction rate constant from the photocatalytic activity of Ag–TiO_2 nanocomposite films.

Table 1. Summary of Ag–TiO_2 nanocomposite films' characterization and photocatalytic activity.

Annealing Temperature	Heating Rate	Crystalline Phase	GMD	Phase Content		Crystallite Size		Relative Thickness	Rate Constant (*k*)
				Anatase	Rutile	Anatase	Rutile		
[°C]	[°C/min]	-	[nm]	[%]	[%]	[nm]	[nm]	-	[1/(h·cm²)]
As-deposited	-	amorphous	13	-	-	-	-	1.00	-
600	3	anatase/rutile	22	85	15	25.9	41.4	0.24	0.079
600	5	anatase/rutile	25	84	16	25.2	30.8	0.25	0.089
600	10	anatase/rutile	24	85	15	29.2	44.8	0.19	0.098
600	30	anatase/rutile	20	87	13	27.3	39.1	0.22	0.104
600	60	anatase/rutile	22	88	12	27.6	32.3	0.38	0.110

3. Materials and Method

3.1. Materials and Experimental Setup

The precursors used were titanium tetraisopropoxide (TTIP, $Ti(OC_3H_7)_4$, Kanto Chemical Co. Inc., Tokyo, Japan) and Ag granules (>99% purity, Kanto Chemical Co. Inc., Tokyo, Japan) to fabricate Ag–TiO_2 nanocomposites. Furthermore, MB, as the model organic pollutant, was subjected to the photocatalytic tests under UV light irradiation. The synthesis method of Ag–TiO_2 nanocomposite thin film was conducted by a one-step aerosol route method implying PECVD and PVD systems. The detailed experimental setup for fabricating Ag–TiO_2 nanocomposite thin films has already been explained in our previous studies [10,20].

Briefly, TTIP vapor was flown and fed continuously to a radio frequency plasma reactor (AX-1000IIP, Adtec Plasma Technology Co. Ltd., Fukuyama, Japan) and dissociated, forming negatively charged TiO_2 nanoparticles [16,26]. Simultaneously, in the evaporation-condensation PVD system, vaporized Ag granules in the tubular furnace (TMF-300N, As One, Tokyo, Japan) were flown by the carrier gas and quickly condensed in the cooling system. The synthesized Ag and TiO_2 nanoparticles were continuously deposited onto a Si substrate with an applied +300 voltage. The voltage was given to uniformly collect the nanoparticles and control the deposition of the nanocomposite [16,26]. To obtain similar 0.35 mg weight s(±5%), the thin film deposition time was varied from 25–30 min. The total pressure of the system was kept at 2–4 kPa by a vacuum pump (SMB-300D, Shinko, Tokyo, Japan). After fabrication, the produced film was then annealed under air. The effect of heating rate was investigated with variation from 3 to 60 °C/min, and the annealing temperature was maintained constant at 600 °C for 12 h.

3.2. Characterization

The surface morphology and film thickness of the nanocomposites with different heating rates were observed by scanning electron microscopy (SEM, S-5200, Hitachi High Technologies, Tokyo, Japan). Furthermore, the geometric mean diameter (GMD) of the nanoparticles can be obtained from the SEM images by measurement of the nanoparticles with Equation (2) [16]:

$$log(\mathrm{GMD}) = \frac{\sum_i^n d_{pi}}{n} \quad (2)$$

The n and d_{pi} in Equation (2) represent the number of nanoparticles measured and the corresponding diameters of nanoparticles, respectively. High-resolution transmission electron microscopy (HRTEM, JEM-2100, JEOL) images were recorded to investigate the morphology of the nanoparticles. Furthermore, nitrogen adsorption–desorption (Autosorb-1, Quantachrome Instruments, Boynton Beach, FL, USA) experiments were conducted to analyze the Brunauer–Emmett–Teller (BET) specific surface area (SBET) and pore volume of the produced nanocomposites after annealing at different heating rates. The samples were degassed at 150 °C prior to nitrogen adsorption–desorption measurements. The relative pressure (P/P_o) adsorption data ranging from 0.05 to 0.3 were used to determine the BET surface area based on a multipoint BET method, while the pore volume was obtained by measuring the nitrogen adsorption volume at a relative pressure (P/P_o) of 0.992.

The crystalline phase, crystallite size, and phase content of anatase and rutile of the nanocomposite were obtained from the XRD (MiniFlex 600, Rigaku, Tokyo, Japan) results. The average crystallite size (D) was calculated by the Scherrer equation in Equation (3):

$$D = \frac{k\,\lambda}{B\cos\theta} \quad (3)$$

k, λ, B, and θ represent the constant value (k = 1.38) [17], the wavelength of the X-ray source (λ = 0.15418 nm), the full-width at half-maximum (FWHM) of the resulted XRD peaks, and the angle of the peak, respectively. In addition, from the XRD pattern results,

the phase content of anatase (W_A) and rutile (W_R) was able to be quantified by applying Equations (4) [2]:

$$W_A = \frac{K_A A_A}{K_A A_A + A_R + K_B A_B}; \; W_R = \frac{A_R}{K_A A_A + A_R + K_B A_B} \quad (4)$$

A_A, A_R, and A_B represent the anatase, rutile, and brookite intensities, respectively. Furthermore, K_A and K_B are the coefficients for anatase (0.886) and brookite (2.721), respectively [2].

3.3. Photocatalytic Test

Photocatalytic test under UV light irradiation was implemented on the Ag–TiO_2 nanocomposite thin film for the degradation of 3 mL MB aqueous solution (2 mg/L) inside a cuvette cell. The calculation of MB degradation efficiency (*MDE*) is shown in Equation (5):

$$MDE = \frac{(C_0 - C_t)}{C_0} \times 100\% \quad (5)$$

C_0 corresponds to the initial concentration, while C_t is the concentration after a certain interval (t), respectively. The concentration of MB before and after irradiation with certain time intervals was measured with UV–Vis spectrophotometry (V-650, Jasco, Tokyo, Japan). From UV–Vis spectrophotometry measurement, the peak absorbance of MB (λ = 664 nm) was known. Furthermore, a calibration curve of MB (MB absorbance = 0.3818 $\times$ MB concentration (mg/L)) was utilized to convert the resulted intensity to the MB concentrations. The rate constant (k) of the photocatalytic activity was obtained from the slope of $\ln (C_0/C_t) = kt$.

4. Conclusions

The influence of the heating rate on the properties and photocatalytic performance of Ag–TiO_2 nanocomposite films were evaluated. Ag-TiO_2 nanocomposite films were prepared by a one-step simultaneous PECVD and PVD system for TiO_2 and Ag nanoparticles, respectively. From the SEM and XRD results, no significant difference was observed in the GMDs, phase content, and crystallite size of the fabricated films at different heating rates, and after annealing, the film consisted of a mixture of anatase–rutile phase (~84% anatase and ~16% rutile). TEM analysis indicated that a high heating rate generated higher crystallinity than that generated at a low heating rate. Nitrogen adsorption–desorption isotherm analysis indicated that the fabricated nanocomposite exhibited a Type II(b) isotherm, indicative of non-porous particles. The BET surface area and total pore volume increased with the heating rate. Furthermore, the photocatalytic activity tested for the degradation of MB under UV light irradiation unveiled that the activity increased with the heating rate. The fabrication of Ag–TiO_2 nanocomposite films by this one-step PECVD and PVD process and subsequent heat treatment with different heating rates means that it is possible to control the properties of the film and influence the increase in the photocatalytic performance.

Supplementary Materials: The following are available online at https://www.mdpi.com/article/10.3390/catal12010017/s1, Figure S1: Schematic of the effect of heat-treatment processes on the fabricated nanocomposite films at different heating rates; Figure S2: Geometric mean diameter (GMD) and relative thickness of the Ag–TiO_2 nanocomposite films annealed at 600 °C at different heating rates from 3 to 60 °C/min including those of the as-deposited film; Figure S3: Selected-area electron diffraction (SAED) patterns of the Ag–TiO_2 nanocomposite films annealed at 600 °C at heating rates of 5 °C/min (a) and 60 °C/min (b). The diffraction peak of anatase (101) is the dominant phase of the nanocomposite films; Figure S4: Crystallite size of Ag–TiO_2 nanocomposite films annealed at 600 °C with heating rates of 3 to 60 °C/min. The crystallite sizes were estimated by the Scherrer equation based on the diffraction peaks of the lattice planes of 101 and 110 of anatase and rutile, respectively; Figure S5: Ag–TiO_2 nanocomposite films' phase content of anatase and rutile mixture at different heating rates. The phase content was estimated using Equation (4) (shown in the manuscript) based

on the diffraction peaks of lattice planes 101 and 110 of anatase and rutile, respectively; Figure S6: UV–Vis absorption of 2 mg/L methylene blue (MB) aqueous solution under UV light irradiation in the presence of the Ag–TiO_2 nanocomposite film annealed at 600 °C with a heating rate of 60 °C/min, respectively; Figure S7: MB degradation efficiency (MDE) of the Ag–TiO_2 nanocomposite films annealed at 600 °C with heating rates of 3 to 60 °C/min. MDE was calculated using Equation (5) (shown in the manuscript).

Author Contributions: Conceptualization, K.K. and M.S.; Methodology, K.K. and D.J.; Formal analysis, K.K., M.H., D.J., and M.K.; Investigation, K.K. and M.K.; Writing—K.K.; Writing—review and editing, K.K., M.H., and M.S.; Supervision: M.S.; Funding acquisition, M.S. and K.K. All authors have read and agreed to the published version of the manuscript.

Funding: This work was supported by the Japan Society for the Promotion of Science [KAKENHI grant; grant number JP21K04750] and was also partly supported by the Hibah PKKM Chemical Engineering Department ITS Surabaya 2021 No. 37/E1/KM.05.01/2021.

Data Availability Statement: The data presented in this study are available on request from the corresponding author.

Acknowledgments: Our sincere gratitude to H. Masuda and M. Ishihara for their assistance in performing the experiments and to M. Maeda for the support in the TEM and SAED analysis.

Conflicts of Interest: The authors declare no conflict of interest.

References

1. Chatterjee, D.; Dasgupta, S. Visible light induced photocatalytic degradation of organic pollutants. *J. Photochem. Photobiol. C Photochem. Rev.* **2005**, *6*, 186–205. [CrossRef]
2. Zhao, C.; Krall, A.; Zhao, H.; Zhang, Q.; Li, Y. Ultrasonic spray pyrolysis synthesis of Ag/TiO_2 nanocomposite photocatalysts for simultaneous H_2 production and CO_2 reduction. *Int. J. Hydrogen Energy* **2012**, *37*, 9967–9976. [CrossRef]
3. Luo, Z.; Poyraz, A.S.; Kuo, C.-H.; Miao, R.; Meng, Y.; Chen, S.-Y.; Jiang, T.; Wenos, C.; Suib, S.L. Crystalline Mixed Phase (Anatase/Rutile) Mesoporous Titanium Dioxides for Visible Light Photocatalytic Activity. *Chem. Mater.* **2015**, *27*, 6–17. [CrossRef]
4. Bumajdad, A.; Madkour, M. Understanding the superior photocatalytic activity of noble metals modified titania under UV and visible light irradiation. *Phys. Chem. Chem. Phys.* **2014**, *16*, 7146–7158. [CrossRef] [PubMed]
5. Galizia, P.; Maizza, G.; Galassi, C. Heating rate dependence of anatase to rutile transformation. *Process. Appl. Ceram.* **2016**, *10*, 235–241. [CrossRef]
6. Dikici, T.; Demirci, S.; Tünçay, M.M.; Yildirim, B.K.; Kaya, N. Effect of heating rate on structure, morphology and photocatalytic properties of TiO2 particles: Thermal kinetic and thermodynamic studies. *J. Sol-Gel Sci. Technol.* **2021**, *97*, 622–637. [CrossRef]
7. Santos, L.M.; Machado, W.A.; França, M.D.; Borges, K.A.; Paniago, R.M.; Patrocinio, A.O.T.; Machado, A.E.H. Structural characterization of Ag-doped TiO2 with enhanced photocatalytic activity. *RSC Adv.* **2015**, *5*, 103752–103759. [CrossRef]
8. Pascariu, P.; Cojocaru, C.; Airinei, A.; Olaru, N.; Rosca, I.; Koudoumas, E.; Suchea, M.P. Innovative Ag–TiO_2 Nanofibers with Excellent Photocatalytic and Antibacterial Actions. *Catalysts* **2021**, *11*, 1234. [CrossRef]
9. Li, R.; Li, T.; Zhou, Q. Impact of Titanium Dioxide (TiO_2) Modification on Its Application to Pollution Treatment—A Review. *Catalysts* **2020**, *10*, 804. [CrossRef]
10. Kusdianto, K.; Jiang, D.; Kubo, M.; Shimada, M. Effect of annealing temperature on the photocatalytic activity of Ag-TiO_2 nanocomposite films by one-step gas-phase deposition. *Mater. Res. Bull.* **2018**, *97*, 497–505. [CrossRef]
11. Mansour, S.A. Non-isothermal crystallization kinetics of nano-sized amorphous TiO_2 prepared by facile sonochemical hydrolysis route. *Ceram. Int.* **2019**, *45*, 2893–2898. [CrossRef]
12. Gunnewiek, R.F.; Kiminami, R.H. Effect of heating rate on microwave sintering of nanocrystalline zinc oxide. *Ceram. Int.* **2014**, *40*, 10667–10675. [CrossRef]
13. Sierra-Uribe, H.; Tuta, E.M.C.; Acevedo-Peña, P. The Effect of the Heating Rate on Anatase Crystal Orientation and Its Impact on the Photoelectrocatalytic Performance of TiO2Nanotube Arrays. *J. Electrochem. Soc.* **2017**, *164*, H279–H285. [CrossRef]
14. Bouhdjer, A.; Attaf, A.; Saidi, H.; Benkhetta, Y.; Aida, M.S.; Bouhaf, I.; Rhil, A. Influence of annealing temperature on In2O3 properties grown by an ultrasonic spray CVD process. *Optik* **2016**, *127*, 6329–6333. [CrossRef]
15. Guhel, Y.; Toloshniak, T.; Bernard, J.; Besq, A.; Germanicus, R.C.; El Fallah, J.; Pesant, J.; Descamps, P.; Boudart, B. Rapid thermal annealing of cerium dioxide thin films sputtered onto silicon (111) substrates: Influence of heating rate on microstructure and electrical properties. *Mater. Sci. Semicond. Process.* **2015**, *30*, 352–360. [CrossRef]
16. Kubo, M.; Mantani, Y.; Shimada, M. Effects of Annealing on the Morphology and Porosity of Porous TiO2 Films Fabricated by Deposition of Aerosol Nanoparticles. *J. Chem. Eng. Jpn.* **2015**, *48*, 292–299. [CrossRef]
17. Ozaki, K.; Hanatani, T.; Nakamura, T. Analysis of crystalline phases in airborne particulates by grazing incidence X-ray diffractometry. *Analyst* **2005**, *130*, 1059–1064. [CrossRef] [PubMed]

18. Gui, M.M.; Wong, W.M.P.; Chai, S.-P.; Mohamed, A.R. One-pot synthesis of Ag-MWCNT@TiO_2 core–shell nanocomposites for photocatalytic reduction of CO2 with water under visible light irradiation. *Chem. Eng. J.* **2015**, *278*, 272–278. [CrossRef]
19. Masuda, Y.; Kato, K. Synthesis and phase transformation of TiO_2 nano-crystals in aqueous solutions. *J. Ceram. Soc. Jpn.* **2009**, *117*, 373–376. [CrossRef]
20. Kusdianto, K.; Jiang, D.; Kubo, M.; Shimada, M. Fabrication of TiO_2–Ag nanocomposite thin films via one-step gas-phase deposition. *Ceram. Int.* **2017**, *43*, 5351–5355. [CrossRef]
21. Tao, C.; Xu, L.; Guan, J. Well-dispersed mesoporous Ta_2O_5 submicrospheres: Enhanced photocatalytic activity by tuning heating rate at calcination. *Chem. Eng. J.* **2013**, *229*, 371–377. [CrossRef]
22. Xiang, Q.; Yu, J.; Cheng, B.; Ong, H.C. Microwave-hydrothermal preparation and visible-light photoactivity of plasmonic photocatalyst Ag-TiO_2 nanocomposite hollow spheres. *Chem. Asian J.* **2010**, *5*, 1466–1674. [CrossRef] [PubMed]
23. Yu, J.; Xiong, J.; Cheng, B.; Liu, S. Fabrication and characterization of Ag–TiO2 multiphase nanocomposite thin films with enhanced photocatalytic activity. *Appl. Catal. B: Environ.* **2005**, *60*, 211–221. [CrossRef]
24. Rouquerol, F.; Rouquerol, J.; Sing, K.; Llewellyn, P.; Maurin, G. *Adsorption by Powders and Porous Solids: Principles, Methodology, and Applications 2014*, 2nd ed.; Elsevier: Oxford, UK, 2014.
25. Sing, K.S.W.; Moscou, L.; Pierotti, R.A.; Rouquerol, J.; Siemieniewska, T. Reporting Physisorption Data for Gas/Solid Systems with Special Reference to the Determination of Surface Area and Porosity. *Pure Appl. Chem.* **1985**, *57*, 603–619. [CrossRef]
26. Kubo, M.; Ishihara, Y.; Mantani, Y.; Shimada, M. Evaluation of the factors that influence the fabrication of porous thin films by deposition of aerosol nanoparticles. *Chem. Eng. J.* **2013**, *232*, 221–227. [CrossRef]